Geophysical Research Letters

RESEARCH LETTER
10.1029/2024GL111929

A Potential Mushy Source for the Geysers of Enceladus and Other Icy Satellites

Colin R. Meyer[1], Jacob J. Buffo[1], Francis Nimmo[2], Andrew J. Wells[3], Samuel Boury[4], Mark Fox-Powell[5], Tara C. Tomlinson[1], Jamie R. G. Parkinson[3], and Geoffrey M. Vasil[6]

[1]Thayer School of Engineering, Dartmouth College, Hanover, NH, USA, [2]Department of Earth & Planetary Sciences, University of California, Santa Cruz, CA, USA, [3]Atmospheric, Oceanic & Planetary Physics, Department of Physics, University of Oxford, Oxford, UK, [4]Université Paris Cité, CNRS, MSC, UMR 7057, Paris, France, [5]AstrobiologyOU, The Open University, Milton Keynes, UK, [6]School of Mathematics, University of Edinburgh, Edinburgh, UK

Abstract Enceladus is a target for astrobiology due to the H_2O plume ejecta measured by the Cassini spacecraft and the inferred subsurface ocean that could be the source of the geysers. Here we explore an alternative where shear heating along tiger stripe fractures produces partial melting in the ice shell and interstitial convection allows fluid to be ejected as geysers. We use an idealized two-dimensional reactive transport model to simulate a mushy region generated by an upper-bound estimate for the localized shear heating rate. We find that the rate of internal melting could potentially match the observed eruption rate. The composition of the liquid brine would be, however, distinct from that of the ocean, due to fractionation during partial melting. This shear heating mechanism for geyser formation could apply to Enceladus and other icy moons and has implications for our understanding of the geophysical processes and astrobiological potential of icy satellites.

Plain Language Summary Enceladus is an icy moon of Saturn that potentially harbors life in the outer solar system. Ice grains erupt out of cracks at the south pole of the moon and the formation mechanism of these geysers is incompletely understood. Here we analyze frictional heating along the cracks and show that salts contained within the ice shell allow the shell to melt at a lower temperature. The melting around the fracture is imperfect and brine flows around ice crystals, which take up only part of the volume. The brine is then able to escape as geysers. We show that the rate of brine production is sufficient to sustain the geysers, although with a potentially different chemistry than the subsurface ocean.

Key Points:

- Shear heating along fractures in the salty ice shell of Enceladus can produce a mushy zone of ice and interstitial brine
- Liquid brine within a mushy region of the shell could be a plume source with sufficient volume and peak melt rates to sustain geysers
- Jets sourced from within the shell may not have a composition representative of the subsurface ocean

Supporting Information:

Supporting Information may be found in the online version of this article.

Correspondence to:

C. R. Meyer,
colin.r.meyer@dartmouth.edu

Citation:

Meyer, C. R., Buffo, J. J., Nimmo, F., Wells, A. J., Boury, S., Fox-Powell, M., et al. (2025). A potential mushy source for the geysers of Enceladus and other icy satellites. *Geophysical Research Letters*, *52*, e2024GL111929. https://doi.org/10.1029/2024GL111929

Received 4 SEP 2024
Accepted 20 JAN 2025

Author Contributions:

Conceptualization: Colin R. Meyer, Jacob J. Buffo, Andrew J. Wells
Data curation: Colin R. Meyer
Formal analysis: Colin R. Meyer, Andrew J. Wells, Geoffrey M. Vasil
Funding acquisition: Colin R. Meyer, Jacob J. Buffo
Investigation: Colin R. Meyer
Methodology: Colin R. Meyer, Jacob J. Buffo, Andrew J. Wells, Samuel Boury, Jamie R. G. Parkinson
Project administration: Colin R. Meyer
Resources: Colin R. Meyer
Software: Colin R. Meyer, Jacob J. Buffo, Andrew J. Wells, Samuel Boury, Jamie R. G. Parkinson
Supervision: Colin R. Meyer
Validation: Colin R. Meyer

1. Introduction

After the discovery of eruptive jets on Saturn's moon Enceladus (Porco et al., 2006), two distinct mechanisms were proposed to explain their origin. First, Nimmo et al. (2007) proposed that tidally driven shear heating along the South Pole fractures causes solid ice to sublimate, generating a vapor source for the plume. Second, Hurford et al. (2007) argued that tidally driven crack opening exposes a subsurface ocean directly to space, later reinforced by Kite and Rubin (2016). It is the second explanation that is now generally favored for three reasons: first, the librations of Enceladus are consistent with the existence of a global liquid ocean (Thomas et al., 2016); second, the plume is modulated on an orbital period, as originally predicted by Hurford et al. (2007) and later corroborated by several groups (Hedman et al., 2013; Ingersoll & Ewald, 2017; Nimmo et al., 2014); and third, a portion of the erupted material is salty (Postberg et al., 2009, 2011). This last observation is the strongest indication of a connection between the subsurface ocean and the eruptive material, as most models assume a salt-free ice shell. Kite and Rubin (2016) showed that turbulent dissipation of tidally driven water within a fracture is sufficient to maintain an open crack from the ocean to the surface. However, Nakajima and Ingersoll (2016) found that refreezing condensation onto the fracture walls above the water level produces thin fractures (~0.1 m wide) that close on timescales of less than a year. Using Cassini Composite Infrared Spectrometer (CIRS) observations, Abramov and Spencer (2009) constrained the width of the fracture zone in a two-dimensional thermal model and found that a narrow crack with a temperature that is far below the melting point of pure ice (i.e., ~225 K crack temperature for their geometry) fits the observed thermal spectrum. Considering the difficulties of fracturing through a ~6 km south polar ice shell (see supplement Text S4 in Supporting Information S1 and Walker et al., 2021) and rapid closure, it is of interest to investigate whether we can find a mechanism explaining the salty jets which does not require direct connection to a subsurface ocean. In this paper, we demonstrate that shear

Visualization: Colin R. Meyer, Andrew J. Wells, Tara C. Tomlinson, Jamie R. G. Parkinson, Geoffrey M. Vasil
Writing – original draft: Colin R. Meyer
Writing – review & editing: Colin R. Meyer, Jacob J. Buffo, Andrew J. Wells, Samuel Boury, Mark Fox-Powell, Tara C. Tomlinson, Jamie R. G. Parkinson, Geoffrey M. Vasil

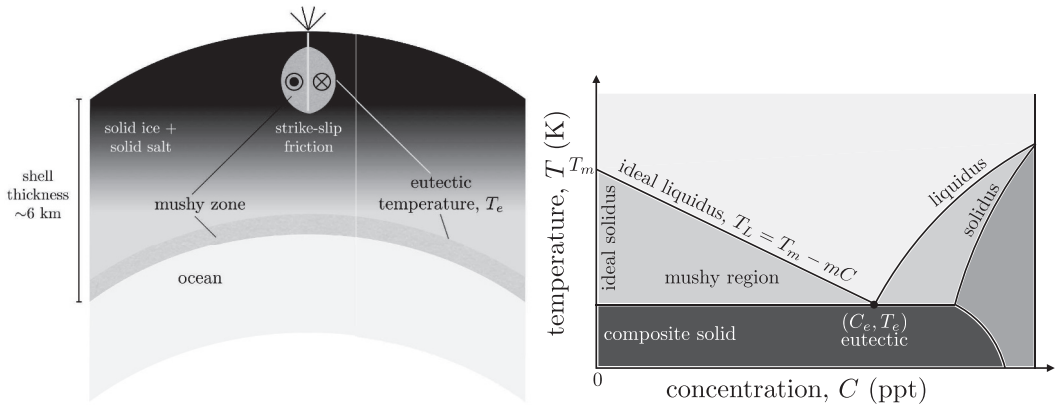

Figure 1. Model for a mushy region around the tiger stripes of Enceladus (left) Schematic for the composition of Enceladus' shell demonstrating strike-slip friction along a tiger stripe fracture. Slip on the finite-length fault varies over time in both directions, although we only depict one direction of the strike-slip motion here. Shear heating on the fracture generates a mushy zone of salty water surrounding ice crystals, providing a liquid source for the geyser material. Darker colors outside of the mushy zone qualitatively correspond to higher expected salt content (Buffo, Meyer, & Parkinson, 2021) (right) Idealized equilibrium phase diagram for a eutectic binary material (e.g., NaCl and H_2O) as a function of temperature and concentration, after Worster (2000).

heating along a tiger stripe fracture in a salty ice shell can induce localized partial melting and could potentially provide an alternative explanation for the observed salty plume particles that does not rely on a direct connection with the ocean.

In many frozen terrestrial and planetary contexts, strike-slip shear heating along narrow zones of deformation efficiently warms the surrounding ice (Golding et al., 2010; Meyer & Minchew, 2018; Nimmo & Gaidos, 2002). By modeling the transport of heat and sublimation vapor flow in a pure ice porous region around a tiger stripe fracture, Nimmo et al. (2007) found a partitioning of sensible and latent heat that explained the vapor transport as well as the thermal anomaly. Observations, however, show that the erupting material consists of a mix of pure and salty ice grains, gases, including water vapor, molecular hydrogen H_2, carbon dioxide CO_2, and methane CH_4, and organic materials (Postberg et al., 2018). Silica nanoparticles were also observed while Cassini was inbound to Saturn, likely to have been sourced ultimately from Enceladus. These observations provided evidence for an oceanic origin for the plume and signatures of water-rock interactions (Hsu et al., 2015; Postberg et al., 2011; Waite et al., 2017). Sublimation cannot produce ice grains with dissolved salts or dust. A liquid source must therefore be responsible for the formation of the geyser ice grains, that is, either a direct connection to the ocean or a reservoir within the shell. Freezing of the shell from a parent ocean could have trapped salt, suspended dust, and incorporated dissolved gases in the shell (Buffo, Meyer, & Parkinson, 2021; Waite et al., 2006, 2017).

Physicochemically heterogeneous materials are common throughout mantles and crusts in planetary geophysics, for example, magma dynamics in the Earth's mantle (Katz, 2008), sea ice growth (Buffo et al., 2018), and marine ice accumulation under ice shelves (Bombosch & Jenkins, 1995). Given the oceanic origin and geophysical reworking of active planetary ice shells (e.g., Europa, Enceladus), a significant and heterogeneous distribution of salt frozen into the shells of these icy satellites is likely (Naseem et al., 2023; Wolfenbarger et al., 2022). Oceanic salt and silica nanoparticles could be incorporated into the ice shell by freezing during Enceladus' formation, or during resurfacing (Buffo, Meyer, & Parkinson, 2021; Buffo, Schmidt, et al., 2021; Hammond et al., 2018). Thinner ice shells will have a larger conductive heat flux and faster growth, since ice that experiences faster growth rates is likely to be saltier than ice that experiences slower growth rates (Buffo, Meyer, & Parkinson, 2021). Entrained salt in the shell means that the melting temperature of the ice is depressed: the impurities in heterogeneous systems facilitate partial melting at lower temperatures than the melting point of pure ice. Shear heating along a tiger stripe fracture could therefore induce partial melting within the shell and generate a near-surface salty liquid source for the south polar plume of Enceladus (Figure 1).

In a multicomponent system, the eutectic temperature T_e is the lowest temperature at which interstitial liquid is stable (Worster, 2000). Given that the ocean temperature is above the eutectic, there is likely a thin mushy zone of salty water surrounding ice crystals at the ice-ocean interface of icy satellite shells (Buffo, Meyer, &

Parkinson, 2021). The minimum depth within the shell where salt exists in a liquid solution is determined by the eutectic temperature, as shown in Figure 1 (left). Figure 1 (right) shows a schematic equilibrium phase diagram for a eutectic binary substance, such as NaCl and H_2O with $T_e = 252$ K. For Enceladus, the rapid loss of heat to outer space leads to near-surface temperatures of about $T_s = 75$ K, that is, below the eutectic, where solid salts can be maintained within the ice shell as a composite phase. At places in the shell where the temperature is above the eutectic (see Figure 1) the salts are dissolved in the interstitial fluid and occupy the pore space around nearly fresh ice crystals. This region is a mushy zone, a region of two-phase coexistence where the liquid and solid phases are in equilibrium, that corresponds to the region between the solidus and liquidus in Figure 1 (right). Close to the fracture, shear heating can warm the ice above the eutectic temperature T_e (viz. Figure 1, left) and form a mushy zone.

2. Methods

We consider the impact of shear heating on a fault with tidally driven back-and-forth strike-slip motion. The shear stress on the fault depends on the friction coefficient μ and the effective normal stress N (overburden weight $\rho_i g z$ less liquid pore pressure p_w, i.e. $N = \rho_i g z - p_w$, where z is the depth below the surface). When melting occurs on the fault, fluid pressure can limit fault stress by lowering the effective normal stress (Rice, 2006). Shear heating $\mu N u$ is given by the shear stress μN multiplied by the slip velocity u (Nielsen et al., 2008). For simplicity, we use a constant overburden stress, rather than a depth-increasing overburden, and do not incorporate the water pressure on the crack face. We do not explicitly quantify the water pressure and it is not clear that the depth-dependence of overburden would be preserved in the effective pressure. In our model, we take the rate of shear heating prior to melting to be the slip velocity u multiplied by the overburden stress, that is, $\mu \rho_i g h u$, where ρ_i the ice density, g the gravity, and h the crack depth (Nimmo & Gaidos, 2002). In effect, our heat flux into the crack is an upper bound on the total potential shear heating. Sliding beneath the fracture is accommodated by viscous deformation but we do not explicitly account for viscous deformation and thermal weakening (e.g., Meyer & Minchew, 2018) in this region. We also use a temporally constant average background heating rate, that is, we do not resolve time variation with tides. This is an acceptable simplification because the heat diffusion timescale is much longer than the orbital timescale. Acknowledging these simplifications, we assume that the friction decreases with added melt according to $\mu(1 - \phi)$ where the porosity ϕ varies along the crack and is solved for in the simulation. The shear heating along the fault f_c is defined as

$$f_c = \mu(1 - \phi)\rho_i g h u. \tag{1}$$

As the porosity grows, the heat flux will decay due to liquid reducing friction along the fault, reducing the heat production.

Following Parkinson et al. (2020), we write the nondimensional temperature θ as

$$\theta = \frac{T - T_e}{\Delta T}, \quad \Delta T = T_L(C_i) - T_e \tag{2}$$

where T_e is the eutectic temperature and $T_L(C_i)$ is the temperature on the liquidus at the initial salt concentration C_i. Here we use the idealized liquidus equation

$$T_L = T_m - mC, \tag{3}$$

where $T_m = 273.15$ K is the pure ice melting temperature and C is the salt concentration (see Figure 1). We scale heights with a characteristic shell thickness $H = 6$ km (within the expected range from Patthoff & Kattenhorn, 2011; Hemingway et al., 2018; Park et al., 2024) and use NaCl parameters with $m = 0.0913$ K/ppt and an initial concentration of $C_i = 2$ parts per thousand (ppt), which is in the range of observations for Enceladus' plume (Postberg et al., 2009) and consistent with a minimum salinity trapped in ice (Buffo et al., 2020; Wolfenbarger et al., 2022). A full table of parameters is given, Table S1 in Supporting Information S1. Our choice of parameters, such as the crack depth and composition, affects the results quantitatively but not qualitatively. In supplement Text S6 in Supporting Information S1, we describe the effects of varying the salinity and ice thickness fraction parameters.

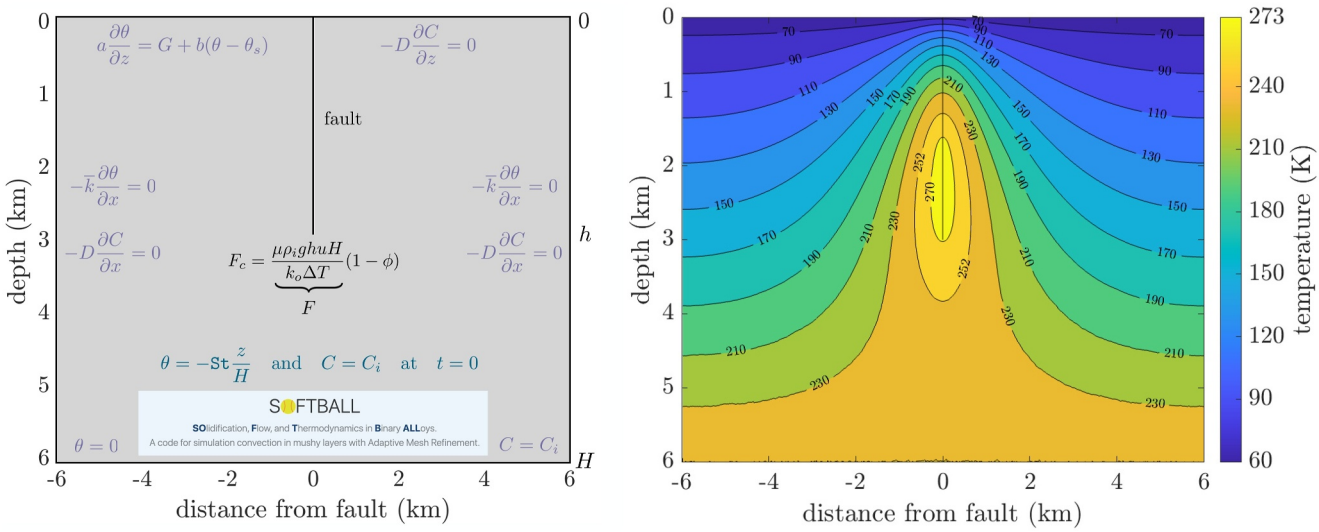

Figure 2. Numerical simulations of mushy zones around a fracture (left) Schematic showing the simulation domain, initial conditions (teal), boundary conditions (purple), and heating along the fracture (black) where θ is dimensionless temperature, ϕ is porosity, C is composition, and $\mathrm{St} = \mathcal{L}/(c_p \Delta T)$ is the Stefan number, with latent heat $\mathcal{L}$ and heat capacity c_p (right) Temperature contours showing the development of a mushy zone ($T \geq T_e = 252$ K) around the fracture (dimensionless heating rate, $F = 280$, corresponding to a slip rate of 3.4 μm/s) and a shell salinity of $C_i = 2$ parts per thousand (ppt), which is consistent with Postberg et al. (2009).

Considering the scales for depth and temperature, we write the constant part of the nondimensional heat flux into the fracture F as

$$F = \frac{\mu \rho_i g h u H}{k_o \Delta T}, \tag{4}$$

where k_o is the thermal conductivity of saltwater. For computational simplicity, we take the thermal conductivity to be independent of temperature. This simplification affects our results quantitatively and constraining the importance of temperature-dependent parameters is an area of future work. The full nondimensional heat flux on the fault (i.e., Equation 1 divided by $k_o \Delta T/H$) is therefore given as

$$F_c = (1-\phi)F. \tag{5}$$

In our simulations, F is the primary control parameter. Taking the parameter values of slip velocity $u = 2.8 \times 10^{-6}$ m s^{-1}, coefficient of friction $\mu = 0.6$ (Golding et al., 2013; Zaman et al., 2024), ice density $\rho_i = 940$ kg m^{-3} (Golden et al., 1998), gravity $g = 0.113$ m s^{-2}, and crack depth $h = 3$ km, we find that $\mu \rho_i g h u = 0.5$ W m^{-2} and $F = 280$ (see Table S1 in Supporting Information S1). Here the value for u is in the range described by Nimmo et al. (2007) and Berne et al. (2023, 2024) and produces the value for F that we use in Figures 2 and 3. The integrated total heat output agrees with Spencer et al. (2018) giving ∼5 GW over an area of 10 km on either side of the 500 km long tiger stripes and an additional ∼0.5 GW comes from latent heat from the plume (Ingersoll & Pankine, 2010).

SOFTBALL (SOlidification, Flow, and Thermodynamics in a Binary ALLoy) is the open-source reactive transport code that we use to solve for temperature, porosity, and salt content as well as fluid flow through the interstices of evolving mushy zones (Adams et al., 2021; Parkinson et al., 2020). We describe the equations for the evolution of a mushy zone in Text S2 in Supporting Information S1 (Fowler, 1985; Hunke et al., 2011; Worster, 2000). In Figure 2, we show the set up of the problem, the key parameters, and the numerically computed temperature field. We consider an isolated fracture in a compositionally homogeneous ice shell (see schematics in Figures 1 and 2). We use an initial shell salinity $C_i = 2$ ppt (Postberg et al., 2009) and consider other shell salinities in the supplement (Figure S8 in Supporting Information S1). We then numerically solve for the

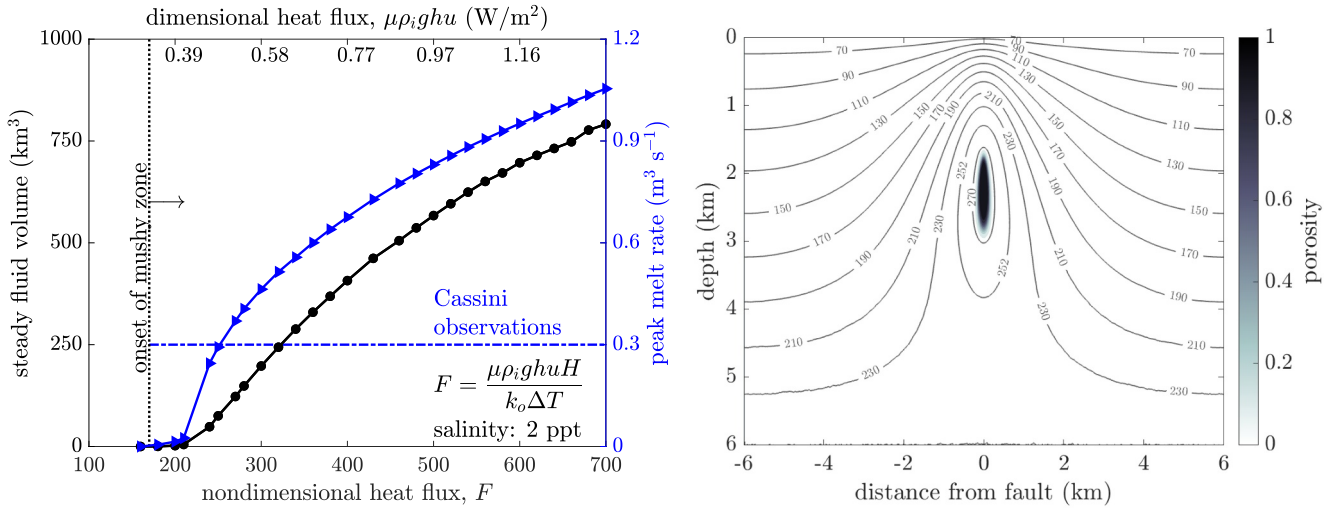

Figure 3. Mushy zone fluid reservoir surrounding tiger stripe fractures with initial shell salinity $C_i = 2$ ppt: (left) Steady interstitial fluid volume and peak melt rate as a function of the shear heat flux into the solid: dimensional on top and nondimensional on bottom. At a critical value of $F \approx 170$, a mushy zone develops around the fracture and this near-surface liquid water can erupt as jets. For larger heat fluxes, the volume of the reservoir and peak melt rate increase (right) Porosity ϕ with superimposed temperature contours from Figure 2 for $F = 280$. The porosity is zero outside the mushy zone, where the temperatures are below the eutectic. The porosity reaches unity along part of the crack. Additional plots for $F = 240$, $F = 300$, and $F = 500$ and other salinities are shown in the supplement (Figures S3 and S8 in Supporting Information S1).

temperature, salinity, and porosity around the fracture using SOFTBALL (see Figure 2). The model conserves mass, salt, energy, and momentum for flow in a reactive porous medium with a porosity dependent permeability. We approximate the densities of ice and water as equal and neglect the viscous deformation of the ice matrix. For the present model, we focus on melt generation and do not include melt extraction along the cracks due to geyser eruptions. We apply a linearized radiative condition at the top of the ice shell (see Text S1 in Supporting Information S1), and insulating conditions on the sides of the domain. We also set the temperature at the eutectic at the bottom of the domain to simulate the top of the ice-ocean interfacial mushy zone. We run the simulations in two dimensions, treating the out-of-plane dimension as invariant along the tiger stripe fractures. The heat flux F_c is implemented via a Gaussian heat source localized at the center of the domain (width $\lesssim$500 m) and a hyperbolic tangent function in the vertical direction (decay away from the crack tip $\lesssim$1,000 m). We initialize the SOFTBALL simulations with a linear temperature profile and a uniformly distributed initial salt concentration ($C_i = 2$ ppt). We then run the simulation to steady state ($\sim$70 kyr; Figure S2 in Supporting Information S1). Additional details on the simulations are included in the supplement Text S2 in Supporting Information S1.

3. Results

We find cold surface temperatures and a warmer mushy zone around the fracture (Figure 2, right). The computed temperature profiles are similar to the results of Kalousová et al. (2016), Hammond (2020), and Stevenson (1996), which are all for a pure ice shell. In Text S1 in Supporting Information S1, we show that the leading-order thermal structure can be understood from steady conduction, with reactive flow modifying the porosity structure, composition and shape of the mushy zone. In SOFTBALL simulations, we find that there is a significant amount of interstitial brine within the mushy zone. Cold, saline brine sinks in the outer part of the mushy zone driving convection, with warmer and fresher fluid rising near the crack (see Figure S4 in Supporting Information S1). This is broadly consistent with a simplified model of buoyant convection in a mushy zone (Boury et al., 2021). The vigor of the convection is characterized by the thermal and compositional Rayleigh numbers (see Text S3 in Supporting Information S1 and Parkinson et al., 2020). Above a critical value, the rising convective flow becomes unstable. Here we follow Boury et al. (2021) and use a small permeability that results in values of the Rayleigh numbers that are below the threshold for instability (see Figure S5 in Supporting Information S1). Near the surface, following the model of Ingersoll and Nakajima (2016), the fluid will boil off and leave the satellite as

geysers that may be fresher than the liquid source (cf. Postberg et al., 2009; Postberg et al., 2011). In addition, bubble formation and bursting near the liquid-space interface could explain the presence of salt-poor, organics-rich ice grains (Postberg et al., 2018). However, we do not explicitly include these processes in the current simulations.

The circulation of brine through the porous ice matrix results in a pooling of salt toward the bottom of the mushy zone, with further drainage prevented in our model by the colder impermeable ice below. This region thus has enhanced phase-weighted salinity, and more easily melts, eventually leading to a region of nearly pure fluid near the bottom of the crack (see Figure 3, right). Accounting for deformation of the ice matrix, it is possible that the pure fluid region could propagate downward as a dike, thereby initiating a connection from the surface to the ocean. In Text S5 in Supporting Information S1, we quantify the timescale for dike propagation based on Lister (1990) and find that it is comparable to but longer than the timescale of our simulations. At the same time, plume eruptions have not been included here and would reduce the volume of melt in the mushy zone, reducing the likelihood of dike formation. At present, our model neglects the potential for sinking of the melt-rich pocket via fracturing or viscous deformation of the surrounding ice (cf. Kalousová et al., 2016) due to the separation of timescales.

We quantify the amount of interstitial water in the mushy zone as the total brine volume

$$v = \ell \int_A \phi \, dS, \tag{6}$$

where ϕ is the melt fraction, $\ell = 500$ km is the total length of the tiger stripe fractures perpendicular to the model domain, and A the area of the domain (see Figure 3). Here we choose ℓ to be the combined length of all four tiger stripe fractures so that our calculations represent the total effects, rather than the dynamics of a single fracture.

The observed flux of ice and vapor from the plume is on the order of 300 kg/s, which is a volume flux of about 0.3 m^3/s (Hansen et al., 2008, 2020; Villanueva et al., 2023). With $F = 280$, the volume is ∼150 km^3 and the observed flux would take about 15 kyr to deplete the reservoir, if no new melting occurred. The volume calculation for $F = 280$ elucidates two important ideas. First, that there is sufficient interstitial brine in the mushy zone surrounding the fracture to account for the plume volume. Second, the volume of material required for the jets is relatively small when compared to the size of the ocean, which is on the order of 20 million km^3 (Spencer & Nimmo, 2013). Thus, it is conceivable that the plume could be maintained without direct access to a large reservoir, such as a subsurface ocean. Thus, the plume on Enceladus and on other icy satellites may be sourced from smaller liquid reservoirs produced by shear heating along faults driven by tidal motion.

From transient simulations, we determine how the liquid volume approaches steady state and we calculate the peak liquid volume production rate (blue, right axis, Figure 3). The peak melt rate estimate for $F = 280$ (slip velocity of $u = 2.8$ μm s^{-1}, see Text S3 in Supporting Information S1) is consistent with the inferred H_2O flux of 0.3 m^3/s and sufficient for E-ring particle source estimates (Ingersoll & Ewald, 2011). Although the melt rate is not necessarily equal to the ejection rate, sufficient melt must be available to replenish the liquid source for eruptions to persist for long periods of time. Here we assume that the dominant impurity is NaCl; the presence of additional impurities with lower eutectic points would likely lead to a larger predicted melt volume and melt production rate, which is something we will explore in future work. In the supplement Text S6.2 in Supporting Information S1, we also present results for varying fracture thicknesses. We find that for very shallow fractures $h = 0.25\,H$, the mushy zone all but vanishes. However, for $h = 0.66\,H$, the mushy zone reaches the base of the ice shell, connecting the surface to the base, which could be an important conduit for life (Hesse et al., 2022).

In Figure 3, smaller values of the nondimensional heat flux imply lower peak melt rates, but can still maintain large volume fluxes for a long time (e.g., ∼8 kyr for $F = 240$). In this case, when the reservoir is depleted the friction on the fault would increase and shear heating would build up a new mushy zone, potentially leading to a long-period oscillation in geyser activity, with a period on the order of the depletion time. This could be analogous to the hypothesis that Enceladus' ocean varies in thickness periodically, due to mismatches in heat output and tidal heat input (Nimmo et al., 2018; Spencer & Nimmo, 2013). Although these simulations represent an upper bound on the rate of shear heating, this mechanism is sufficient to explain the observed geyser ejection rate and required

brine volume. Similarly, the shear heating mechanism could potentially explain the inference of sporadic jets on Europa (e.g., Roth et al., 2014), as tectonic activity could result in a short-lived plume sourced from a mushy zone.

4. Discussion

Observations show that the plume brightness varies diurnally with a phase lag (Hedman et al., 2018; Nimmo et al., 2014; Porco et al., 2014), which is consistent with Hurford et al. (2007). As normal stresses on the faults change into a more tensile state due to tides, the brightness of the plume also changes (Berne et al., 2024). As the cracks open up, more material is able to come up from the fluid reservoir and emanate out as the jets. Here we postulate that the reservoir is not necessarily a subsurface ocean, but could instead be a mushy zone within the ice shell. A connection from the surface to a reservoir is still required, but it is not necessary for the fracture to extend all the way through the ice shell. The lag from the tidal variation observed by Nimmo et al. (2014) is still consistent with this mechanism so long as the opening of the fractures allows material to emerge, just as in the Hurford et al. (2007) model. Moreover, the mushy zone would naturally generate a low-viscosity region around the tiger stripes that Běhounková et al. (2015) used to explain the phase lag. Kite and Rubin (2016) proposed that tides periodically push the crack faces together causing the fluid to rise turbulently. However, the tidal squeezing implied by their model is difficult to reconcile because the jets are still active during the full tidal cycle. Due to the salts in the shell, a mushy zone around the tiger stripes will likely form in the Kite and Rubin (2016) model because of the turbulent heat flux on the crack walls.

The double ridges observed around the tiger stripe fractures on the south pole of Enceladus (G. W. Patterson et al., 2018) and in many places on Europa may provide an additional line of evidence suggesting that shear heating along the fractures produces internal melting. Culberg et al. (2022) describe double-ridge formation on icy satellites building on evidence from refreezing in the surface snow of the Greenland Ice Sheet. As liquid water freezes in a near-surface reservoir, it expands and drives the sides of the crack vertically. The mushy zone that we propose could be a near-surface water source and the double ridges could be evidence for episodic geysering followed by refreezing dormant periods. Triton is another place where double ridges may be associated with shear heating (Prockter et al., 2005).

Cassini's detection of molecular hydrogen H_2 is a strong indicator of water-rock interactions on the seafloor, favoring an ocean source for the plume. Since the H_2 residence time in the ocean is less than 1 million years, Waite et al. (2017) concludes that H_2 must be produced on Enceladus. Alternatively, molecular hydrogen H_2 could be trapped in clathrates with stabilization from CH_4 and CO_2 (Waite et al., 2017) or persist as entrained gas bubbles within the ice shell, as found in ice sheets on Earth (Bender et al., 1997). Waite et al. (2017) argue that the hydrogen cannot be sourced from clathrates within the shell of Enceladus because the ratio of H_2 to CO_2 and CH_4 is too large. Yet, given the volatility of H_2, partial melting could allow some of the hydrogen to escape while leaving the carbon dioxide and methane behind. Gas release during terrestrial ice core decompression show signs of this effect (Gow & Williamson, 1975), but targeted experiments could test this hypothesis. Substantial depletion of H_2 in the ice shell by diffusion is also unlikely: laboratory evidence shows that the diffusion of H_2 through ice at Earth temperatures (with diffusivity $D_{H_2} \sim 10^{-11}$ m^2 s^{-1}) is at least an order of magnitude smaller than the first-order estimate of the diffusivity $D \sim h^2/t \sim 2.5 \times 10^{-10}$ m^2 s^{-1} required for gas to escape from an $h \sim 6$ km shell in $t_{age} \sim 4.5$ billion years. The diffusivity D_{H_2} is likely even smaller at Enceladus temperatures (J. D. Patterson & Saltzman, 2021), further reducing the possibility of substantial diffusive escape of H_2. Here we propose that partial melting of a clathrate within the shell could (a) produce sufficient volume of H_2 to match the observed ejection rate of $\sim 10^9$ mol H_2/year and (b) that the H_2 may escape without bringing all of the CO_2 and CH_4. We envision that ice flow, refreezing, and tectonic reorganization of the shell will resupply salty ice and clathrates to the mushy zone, maintaining the plume composition.

With a mushy zone sourcing the plume material, the salt, nanoparticles, and gas clathrates would need to be replenished over time in order to maintain the levels observed by Cassini. Although we do not model the replenishment processes here, it is an area of future work. Melting and plume ejection at the tiger stripes will thin the shell in the south pole, causing ice from northern latitudes to flow down. The shell material that flows into the south pole will not be depleted of salts, nanoparticles, and gas clathrates. In addition, our modeled salinity is larger than the observed ice grain salinity. Vapor condensation onto grains is almost certainly occurring within the plume environment before ejection into space (Postberg et al., 2009, 2011, 2018; Schmidt et al., 2008) which could act to dilute the concentration of salts within individual grains. In

this case, boiling of the liquid and a small amount of salt would increase the mushy zone salinity, leading to dissolution of the ice crystals and potentially gas clathrates, which will draw in additional liquid and gas into the mushy reservoir. The liquid-source temperature in the mushy region (~270 K, cf. Figure 2) is sufficient for grain collisions in the conduit carrying material from within the shell into space (Brilliantov et al., 2008; Schmidt et al., 2008). For large fracture fractions, our results show that the mushy zone may periodically form a dike down to the ocean, potentially leading to the formation of an ocean-surface conduit that could source the geysers. Then, shear heating will generate a new mushy zone in a region of the shell that is not depleted of salts and other contaminants. We will test these ideas in future work.

Within the mushy zone generated by the shear heating mechanism, the source brine is concentrated interstitial liquid produced from the remelting of the ice shell. Thus, it may not be representative of the underlying ocean chemistry (see Figure S6 in Supporting Information S1). The difference between interstitial brine and the ocean has fundamental implications for how we relate observed plume properties to interior liquid water reservoirs. Cryoconcentrative processes in the shell and ion fractionation during droplet solidification may result in plume compositions that vary significantly from that of the shell or ocean (Buffo et al., 2023; Buffo, Meyer, & Parkinson, 2021; Fox-Powell & Cousins, 2021). Such uncertainties feed into predictions of ocean geochemistry and habitability based on observed plume compositions. We suggest caution in extrapolating plume properties to interior ocean properties. Without corroborating evidence of a direct ocean-to-surface conduit, the plume may be sourced from an intrashell brine reservoir whose composition and concentration will depend on the geophysical history and dynamics of the hydrologic body and surrounding ice shell.

In reconsidering the Nimmo et al. (2007) shear heating theory, we now include salts and the formation of a mushy zone. These additional processes fix some of the issues with the original theory and solve some of the puzzles about the ocean source mechanism. However, other pieces require further investigation, such as hydrogen gas, nanoparticles, and the boiling process. Currently, none of these is a roadblock to the theory and future work will determine the process that controls geyser formation at Enceladus and other icy satellites. As an example of an area where further work is required, the conditions at the outlet of the jets play a fundamental role in the observed signal, independent of whether it is a mushy or ocean source (Fifer et al., 2022; Ingersoll & Nakajima, 2016; Mitchell et al., 2024). More focused effort in this area would help us understand the Cassini observations as well as the ocean and/or shell properties. In terms of molecular hydrogen, focused lab work about partial melting of clathrates and boiling of gas-containing liquids would elucidate the possible configurations that allow for the observed H_2/CH_4-CO_2 ratios.

5. Conclusions

We described the potential for a mushy source for the geysers of Enceladus, by revisiting the Nimmo et al. (2007) idea that shear heating along the tiger stripes is responsible for the jet material. Instead of treating the shell as pure ice, we considered a composite of solid ice and salt, which would naturally form when freezing a salty ocean. Using an idealized model, we demonstrated that shear heating along the tiger stripe fractures can generate a mushy zone at depth, while maintaining cold surface temperatures, in line with Abramov and Spencer (2009). Within the mushy zone, we found that there is sufficient liquid volume in the interstices to source the volume of observed geyser material and that the melting rate can match the geyser ejection rate. However, the composition of the liquid brine within the mushy zone may be distinct from that of the ocean. Our simulations represent a glimpse at an alternative possibility for the source of the geysers on Enceladus and other icy satellites. For example, the hints at a plume on Europa could come from a transient source such as shear heating in a mushy zone. Our theory describes a general mechanism that should apply to all tectonically active icy satellites.

Conflict of Interest

The authors declare no conflicts of interest relevant to this study.

Data Availability Statement

We did not use any observational data in this paper beyond the geyser flux estimates (Hansen et al., 2008, 2020; Villanueva et al., 2023) and model outputs by Berne et al. (2023, 2024). The SOFTBALL code and its associated documentation can be found in Parkinson et al. (2020).

Acknowledgments
We thank Bill McKinnon, Alan Rempel, Aleah Sommers, and John Spencer for insightful conversations. This work was supported by NASA (80NSSC21M0329, 80NSSC21K1804); ARO (78811EG); and the Neukom Institute at Dartmouth College. Thanks to Editor Kevin Lewis and two anonymous reviewers.

References

Abramov, O., & Spencer, J. R. (2009). Endogenic heat from Enceladus' south polar fractures: New observations, and models of conductive surface heating. *Icarus*, *199*(1), 189–196. https://doi.org/10.1016/j.icarus.2008.07.016

Adams, M., Colella, P., Graves, D. T., Johnson, J. N., Keen, N. D., Ligocki, T. J., et al. (2021). Chombo software package for AMR applications - Design document (Tech. Rep.). *Berkeley, CA: Lawrence Berkeley National Laboratory, LBNL-6616E*.

Běhounková, M., Tobie, G., Čadek, O., Choblet, G., Porco, C., & Nimmo, F. (2015). Timing of water plume eruptions on Enceladus explained by interior viscosity structure. *Nature Geoscience*, *8*(8), 601–604. https://doi.org/10.1038/ngeo2475

Bender, M., Sowers, T., & Brook, E. (1997). Gases in ice cores. *Proceedings of the National Academy of Sciences of the United States of America*, *94*(16), 8343–8349. https://doi.org/10.1073/pnas.94.16.8343

Berne, A., Simons, M., Keane, J. T., Leonard, E. J., & Park, R. S. (2024). Jet activity on Enceladus linked to tidally driven strike-slip motion along tiger stripes. *Nature Geoscience*, *17*(5), 1–7. https://doi.org/10.1038/s41561-024-01418-0

Berne, A., Simons, M., Keane, J. T., & Park, R. S. (2023). Inferring the mean thickness of the outer ice shell of Enceladus from diurnal crustal deformation. *Journal of Geophysical Research*, *128*(6), e2022JE007712. https://doi.org/10.1029/2022JE007712

Bombosch, A., & Jenkins, A. (1995). Modeling the formation and deposition of frazil ice beneath Filchner-Ronne Ice Shelf. *Journal of Geophysical Research*, *100*(C4), 6983–6992. https://doi.org/10.1029/94JC03224

Boury, S., Meyer, C. R., Vasil, G. M., & Wells, A. J. (2021). Convection in a mushy layer along a vertical heated wall. *Journal of Fluid Mechanics*, *926*, A33. https://doi.org/10.1017/jfm.2021.742

Brilliantov, N. V., Schmidt, J., & Spahn, F. (2008). Geysers of Enceladus: Quantitative analysis of qualitative models. *Planetary and Space Science*, *56*(12), 1596–1606. https://doi.org/10.1016/j.pss.2008.06.007

Buffo, J. J., Meyer, C. R., Chivers, C. J., Walker, C. C., Huber, C., & Schmidt, B. E. (2023). Geometry of freezing impacts ice composition: Implications for icy satellites. *Journal of Geophysical Research*, *128*(3), e2022JE007389. https://doi.org/10.1029/2022JE007389

Buffo, J. J., Meyer, C. R., & Parkinson, J. R. G. (2021). Dynamics of a solidifying icy satellite shell. *Journal of Geophysical Research*, *126*(5), e2020JE006741. https://doi.org/10.1029/2020JE006741

Buffo, J. J., Schmidt, B. E., & Huber, C. (2018). Multiphase reactive transport and platelet ice accretion in the sea ice of McMurdo Sound, Antarctica. *Journal of Geophysical Research*, *123*(1), 324–345. https://doi.org/10.1002/2017JC013345

Buffo, J. J., Schmidt, B. E., Huber, C., & Meyer, C. R. (2021). Characterizing the ice-ocean interface of icy worlds: A theoretical approach. *Icarus*, *360*, 114318. https://doi.org/10.1016/j.icarus.2021.114318

Buffo, J. J., Schmidt, B. E., Huber, C., & Walker, C. C. (2020). Entrainment and dynamics of ocean-derived impurities within Europa's ice shell. *Journal of Geophysical Research*, *125*(10), e2020JE006394. https://doi.org/10.1029/2020JE006394

Culberg, R., Schroeder, D. M., Walker, M., & Steinbr ugge, G. (2022). Double ridge formation over shallow water sills on Jupiter's moon Europa. *Nature Communications*, *13*(2007), 1723–2041. https://doi.org/10.1038/s41467-022-29458-3

Fifer, L. M., Catling, D. C., & Toner, J. D. (2022). Chemical fractionation modeling of plumes indicates a gas-rich, moderately alkaline Enceladus ocean. *Planet. Sci. J.*, *3*(8), 191. https://doi.org/10.3847/PSJ/ac7a9f

Fowler, A. C. (1985). The formation of freckles in binary alloys. *IMA Journal of Applied Mathematics*, *35*(2), 159–174. https://doi.org/10.1093/imamat/35.2.159

Fox-Powell, M. G., & Cousins, C. R. (2021). Partitioning of crystalline and amorphous phases during freezing of simulated Enceladus ocean fluids. *Journal of Geophysical Research*, *126*(1), e2020JE006628. https://doi.org/10.1029/2020JE006628

Golden, K. M., Ackley, S. F., & Lytle, V. I. (1998). The percolation phase transition in sea ice. *Science*, *282*(5397), 2238–2241. https://doi.org/10.1126/science.282.5397.2238

Golding, N., Burks, C. E., Lucas, K. N., Fortt, A. L., Snyder, S. A., & Schulson, E. M. (2013). Mechanical properties of the ice i–magnesium sulfate eutectic: A comparison with freshwater ice in reference to Europa. *Icarus*, *225*(1), 248–256. https://doi.org/10.1016/j.icarus.2013.02.037

Golding, N., Schulson, E. M., & Renshaw, C. E. (2010). Shear faulting and localized heating in ice: The influence of confinement. *Acta Materialia*, *58*(15), 5043–5056. https://doi.org/10.1016/j.actamat.2010.05.040

Gow, A. J., & Williamson, T. (1975). Gas inclusions in the Antarctic ice sheet and their glaciological significance. *Journal of Geophysical Research*, *80*(36), 5101–5108. https://doi.org/10.1029/JC080i036p05101

Hammond, N. P. (2020). Estimating the magnitude of cyclic slip on strike-slip faults on Europa. *Journal of Geophysical Research*, *125*(7), e2019JE006170. https://doi.org/10.1029/2019JE006170

Hammond, N. P., Parmentier, E. M., & Barr, A. C. (2018). Compaction and melt transport in ammonia-rich ice shells: Implications for the evolution of Triton. *Journal of Geophysical Research*, *123*(12), 3105–3118. https://doi.org/10.1029/2018JE005781

Hansen, C. J., Esposito, L. W., Colwell, J. E., Hendrix, A. R., Portyankina, G., Stewart, A. I. F., & West, R. A. (2020). The composition and structure of Enceladus' plume from the complete set of Cassini UVIS occultation observations. *Icarus*, *344*, 113461. https://doi.org/10.1016/j.icarus.2019.113461

Hansen, C. J., Esposito, L. W., Stewart, A. I. F., Meinke, B., Wallis, B., Colwell, J. E., et al. (2008). Water vapour jets inside the plume of gas leaving Enceladus. *Nature*, *456*(7221), 477–479. https://doi.org/10.1038/nature07542

Hedman, M. M., Dhingra, D., Nicholson, P. D., Hansen, C. J., Portyankina, G., Ye, S., & Dong, Y. (2018). Spatial variations in the dust-to-gas ratio of Enceladus' plume. *Icarus*, *305*, 123–138. https://doi.org/10.1016/j.icarus.2018.01.006

Hedman, M. M., Gosmeyer, C. M., Nicholson, P. D., Sotin, C., Brown, R. H., Clark, R. N., et al. (2013). An observed correlation between plume activity and tidal stresses on Enceladus. *Nature*, *500*(7461), 182–184. https://doi.org/10.1038/nature12371

Hemingway, D., Iess, L., Tajeddine, R., & Tobie, G. (2018). The interior of Enceladus. In P. M. Schenk, R. N. Clark, C. J. A. Howett, A. J. Verbiscer, & J. H. Waite (Eds.), *Enceladus and the icy moons of Saturn* (pp. 57–78). University of Arizona Press. https://doi.org/10.2307/j.ctv65sw2b.12

Hesse, M. A., Jordan, J. S., Vance, S. D., & Oza, A. V. (2022). Downward oxidant transport through Europa's ice shell by density-driven brine percolation. *Geophysical Research Letters*, *49*(5), e2021GL095416. https://doi.org/10.1029/2021GL095416
Hsu, H.-W., Postberg, F., Sekine, Y., Shibuya, T., Kempf, S., Horányi, M., et al. (2015). Ongoing hydrothermal activities within Enceladus. *Nature*, *519*(7542), 207–210. https://doi.org/10.1038/nature14262
Hunke, E. C., Notz, D., Turner, A. K., & Vancoppenolle, M. (2011). The multiphase physics of sea ice: A review for model developers. *The Cryosphere*, *5*(4), 989–1009. https://doi.org/10.5194/tc-5-989-2011
Hurford, T. A., Helfenstein, P., Hoppa, G. V., Greenberg, R., & Bills, B. G. (2007). Eruptions arising from tidally controlled periodic openings of rifts on Enceladus. *Nature*, *447*(7142), 292–294. https://doi.org/10.1038/nature05821
Ingersoll, A. P., & Ewald, S. P. (2011). Total particulate mass in Enceladus plumes and mass of Saturn's E ring inferred from Cassini ISS images. *Icarus*, *216*(2), 492–506. https://doi.org/10.1016/j.icarus.2011.09.018
Ingersoll, A. P., & Ewald, S. P. (2017). Decadal timescale variability of the Enceladus plumes inferred from Cassini images. *Icarus*, *282*, 260–275. https://doi.org/10.1016/j.icarus.2016.09.018
Ingersoll, A. P., & Nakajima, M. (2016). Controlled boiling on Enceladus. 2. model of the liquid-filled cracks. *Icarus*, *272*, 319–326. https://doi.org/10.1016/j.icarus.2015.12.040
Ingersoll, A. P., & Pankine, A. A. (2010). Subsurface heat transfer on Enceladus: Conditions under which melting occurs. *Icarus*, *206*(2), 594–607. https://doi.org/10.1016/j.icarus.2009.09.015
Kalousová, K., Souček, O., Tobie, G., Choblet, G., & Čadek, O. (2016). Water generation and transport below Europa's strike-slip faults. *Journal of Geophysical Research*, *121*(12), 2444–2462. https://doi.org/10.1002/2016JE005188
Katz, R. F. (2008). Magma dynamics with the enthalpy method: Benchmark solutions and magmatic focusing at mid-ocean ridges. *Journal of Petrology*, *49*(12), 2099–2121. https://doi.org/10.1093/petrology/egn058
Kite, E. S., & Rubin, A. M. (2016). Sustained eruptions on Enceladus explained by turbulent dissipation in tiger stripes. *Proceedings of the National Academy of Sciences*, *113*(15), 3972–3975. https://doi.org/10.1073/pnas.1520507113
Lister, J. R. (1990). Buoyancy-driven fluid fracture: Similarity solutions for the horizontal and vertical propagation of fluid-filled cracks. *Journal of Fluid Mechanics*, *217*, 213–239. https://doi.org/10.1017/S0022112090000696
Meyer, C. R., & Minchew, B. M. (2018). Temperate ice in the shear margins of the Antarctic ice sheet: Controlling processes and preliminary locations. *Earth and Planetary Science Letters*, *498*, 17–26. https://doi.org/10.1016/j.epsl.2018.06.028
Mitchell, K. L., Rabinovitch, J., Scamardella, J. C., & Cable, M. L. (2024). A proposed model for cryovolcanic activity on Enceladus driven by volatile exsolution. *Journal of Geophysical Research*, *129*(7), e2023JE007977. https://doi.org/10.1029/2023JE007977
Nakajima, M., & Ingersoll, A. P. (2016). Controlled boiling on Enceladus. 1. model of the vapor-driven jets. *Icarus*, *272*, 309–318. https://doi.org/10.1016/j.icarus.2016.02.027
Naseem, M., Neveu, M., Howell, S., Lesage, E., Daswani, M. M., & Vance, S. D. (2023). Salt distribution from freezing intrusions in ice shells on ocean worlds: Application to Europa. *Planet. Sci. J.*, *4*(9), 181. https://doi.org/10.3847/PSJ/ace5a2
Nielsen, S., Di Toro, G., Hirose, T., & Shimamoto, T. (2008). Frictional melt and seismic slip. *Journal of Geophysical Research*, *113*(B1). https://doi.org/10.1029/2007JB005122
Nimmo, F., Barr, A. C., Běhounková, M., & McKinnon, W. B. (2018). The thermal and orbital evolution of Enceladus: Observational constraints and models. In P. M. Schenk, R. N. Clark, C. J. A. Howett, A. J. Verbiscer, & J. H. Waite (Eds.), *Enceladus and the icy moons of Saturn* (pp. 79–94). University of Arizona Press. https://doi.org/10.2307/j.ctv65sw2b.13
Nimmo, F., & Gaidos, E. (2002). Strike-slip motion and double ridge formation on Europa. *Journal of Geophysical Research*, *107*(E4), 5–8. https://doi.org/10.1029/2000JE001476
Nimmo, F., Porco, C., & Mitchell, C. (2014). Tidally modulated eruptions on Enceladus: Cassini ISS observations and models. *The Astronomical Journal*, *148*(3), 46. https://doi.org/10.1088/0004-6256/148/3/46
Nimmo, F., Spencer, J. R., Pappalardo, R. T., & Mullen, M. E. (2007). Shear heating as the origin of the plumes and heat flux on Enceladus. *Nature*, *447*(7142), 289–291. https://doi.org/10.1038/nature05783
Park, R. S., Mastrodemos, N., Jacobson, R. A., Berne, A., Vaughan, A. T., Hemingway, D. J., et al. (2024). The global shape, gravity field, and libration of Enceladus. *Journal of Geophysical Research*, *129*(1), e2023JE008054. https://doi.org/10.1029/2023JE008054
Parkinson, J. R. G., Martin, D. F., Wells, A. J., & Katz, R. F. (2020). Modelling binary alloy solidification with adaptive mesh refinement. *Journal of Computational Physics*, *5*, 100043. https://doi.org/10.1016/j.jcpx.2019.100043
Patterson, G. W., Kattenhorn, S. A., Helfenstein, P., Collins, G. C., & Pappalardo, R. T. (2018). The interior of Enceladus. In P. M. Schenk, R. N. Clark, C. J. A. Howett, A. J. Verbiscer, & J. H. Waite (Eds.), *Enceladus and the icy moons of Saturn* (p. 95). University of Arizona Press. https://doi.org/10.2307/j.ctv65sw2b.12
Patterson, J. D., & Saltzman, E. S. (2021). Diffusivity and solubility of H2 in ice Ih: Implications for the behavior of H2 in polar ice. *Journal of Geophysical Research*, *126*(10), e2020JD033840. https://doi.org/10.1029/2020JD033840
Patthoff, D. A., & Kattenhorn, S. A. (2011). A fracture history on Enceladus provides evidence for a global ocean. *Geophysical Research Letters*, *38*(18). https://doi.org/10.1029/2011GL048387
Porco, C., DiNino, D., & Nimmo, F. (2014). How the geysers, tidal stresses, and thermal emission across the south polar terrain of Enceladus are related. *The Astronomical Journal*, *148*(3), 45. https://doi.org/10.1088/0004-6256/148/3/45
Porco, C., Helfenstein, P., Thomas, P. C., Ingersoll, A. P., Wisdom, J., West, R., et al. (2006). Cassini observes the active south pole of Enceladus. *Science*, *311*(5766), 1393–1401. https://doi.org/10.1126/science.1123013
Postberg, F., Kempf, S., Schmidt, J., Brilliantov, N., Beinsen, A., Abel, B., et al. (2009). Sodium salts in E-ring ice grains from an ocean below the surface of Enceladus. *Nature*, *459*(7250), 1098–1101. https://doi.org/10.1038/nature08046
Postberg, F., Khawaja, N., Abel, B., Choblet, G., Glein, C. R., Gudipati, M. S., et al. (2018). Macromolecular organic compounds from the depths of Enceladus. *Nature*, *558*(7711), 564–568. https://doi.org/10.1038/s41586-018-0246-4
Postberg, F., Schmidt, J., Hillier, J., Kempf, S., & Srama, R. (2011). A salt-water reservoir as the source of a compositionally stratified plume on Enceladus. *Nature*, *474*(7353), 620–622. https://doi.org/10.1038/nature10175
Prockter, L. M., Nimmo, F., & Pappalardo, R. T. (2005). A shear heating origin for ridges on Triton. *Geophysical Research Letters*, *32*(14). https://doi.org/10.1029/2005GL022832
Rice, J. R. (2006). Heating and weakening of faults during earthquake slip. *Journal of Geophysical Research*, *111*(B5). https://doi.org/10.1029/2005JB004006
Roth, L., Saur, J., Retherford, K. D., Strobel, D. F., Feldman, P. D., McGrath, M. A., & Nimmo, F. (2014). Transient water vapor at Europa's south pole. *Science*, *343*(6167), 171–174. https://doi.org/10.1126/science.1247051
Schmidt, J., Brilliantov, N., Spahn, F., & Kempf, S. (2008). Slow dust in Enceladus' plume from condensation and wall collisions in tiger stripe fractures. *Nature*, *451*(7179), 685–688. https://doi.org/10.1038/nature06491

Spencer, J. R., & Nimmo, F. (2013). Enceladus: An active ice world in the Saturn system. *Annual Review of Earth and Planetary Sciences*, *41*(1), 693–717. https://doi.org/10.1146/annurev-earth-050212-124025

Spencer, J. R., Nimmo, F., Ingersoll, A. P., Hurford, T. A., Kite, E. S., Rhoden, A. R., et al. (2018). Plume origins and plumbing: From ocean to surface. In P. M. Schenk, R. N. Clark, C. J. A. Howett, A. J. Verbiscer, & J. H. Waite (Eds.), *Enceladus and the icy moons of Saturn* (pp. 163–174). University of Arizona Press. https://doi.org/10.2307/j.ctv65sw2b.18

Stevenson, D. J. (1996). Heterogeneous tidal deformation and geysers on Europa. In *Europa ocean conference* (pp. 69–70). San Juan Capistrano.

Thomas, P. C., Tajeddine, R., Tiscareno, M. S., Burns, J. A., Joseph, J., Loredo, T. J., et al. (2016). Enceladus's measured physical libration requires a global subsurface ocean. *Icarus*, *264*, 37–47. https://doi.org/10.1016/j.icarus.2015.08.037

Villanueva, G. L., Hammel, H. B., Milam, S. N., Kofman, V., Faggi, S., Glein, C. R., et al. (2023). JWST molecular mapping and characterization of Enceladus' water plume feeding its torus. *Nature Astronomy*, *7*(9), 1–7. https://doi.org/10.1038/s41550-023-02009-6

Waite, J. H., Combi, M. R., Ip, W.-H., Cravens, T. E., McNutt, R. L., Kasprzak, W., et al. (2006). Cassini ion and neutral mass spectrometer: Enceladus plume composition and structure. *Science*, *311*(5766), 1419–1422. https://doi.org/10.1126/science.1121290

Waite, J. H., Glein, C. R., Perryman, R. S., Teolis, B. D., Magee, B. A., Miller, G., et al. (2017). Cassini finds molecular hydrogen in the Enceladus plume: Evidence for hydrothermal processes. *Science*, *356*(6334), 155–159. https://doi.org/10.1126/science.aai8703

Walker, C. C., Bassis, J. N., & Schmidt, B. E. (2021). Propagation of vertical fractures through planetary ice shells: The role of basal fractures at the ice–ocean interface and proximal cracks. *Planet. Sci. J.*, *2*(4), 135. https://doi.org/10.3847/PSJ/ac01ee

Wolfenbarger, N. S., Buffo, J. J., Soderlund, K. M., & Blankenship, D. D. (2022). Ice shell structure and composition of ocean worlds: Insights from accreted ice on Earth. *Astrobiology*, *22*(8), 937–961. https://doi.org/10.1089/ast.2021.0044

Worster, M. G. (2000). Solidification of fluids. In G. K. Batchelor, H. K. Moffatt, & M. G. Worster (Eds.), *Perspectives in fluid dynamics* (pp. 393–444). Cambridge University Press.

Zaman, M., McCarthy, C., Skarbek, R. M., & Savage, H. M. (2024). Frictional strength, stability, and potential shear heating on icy satellite faults. *Journal of Geophysical Research*, *129*(3), e2023JE008215. https://doi.org/10.1029/2023JE008215

References From the Supporting Information

Broberg, K. B. (1999). *Cracks and fracture*. Academic Press.

Crawford, G. D., & Stevenson, D. J. (1988). Gas-driven water volcanism in the resur– facing of Europa. *Icarus*, *73*(1), 66–79. https://doi.org/10.1016/0019-1035(88)90085-1

Hansen, C. J., Esposito, L., Stewart, A. I. F., Colwell, J., Hendrix, A., Pryor, W., & West, R. (2006). Enceladus' water vapor plume Enceladus' water vapor plume. *Science*, *311*(5766), 1422–1425. https://doi.org/10.1126/science.1121254

Hemingway, D. J., Rudolph, M. L., & Manga, M. (2020). Cascading parallel fractures on Enceladus. *Nature Astronomy*, *4*(3), 234–239. https://doi.org/10.1038/s41550-019-0958-x

Kang, W., Mittal, T., Bire, S., Campin, J. M., & Marshall, J. (2022). How does salinity shape ocean circulation and ice geometry on Enceladus and other icy satellites? *Science Advances*, *8*(29), eabm4665. https://doi.org/10.1126/sciadv.abm4665

Katz, R. F., & Worster, M. G. (2008). Simulation of directional solidification, thermo– chemical convection, and chimney formation in a Hele-Shaw cell. *Journal of Computational Physics*, *227*(23), 9823–9840. https://doi.org/10.1016/j.jcp.2008.06.039

Nimmo, F., Bills, B. G., & Thomas, P. C. (2011). Geophysical implications of the long– wavelength topography of the Saturnian satellites. *Journal of Geophysical Research*, *116*(E11), E11001. https://doi.org/10.1029/2011JE003835

Nye, J. F. (1955). Comments on Dr. Loewe's letter and notes on crevasses. *Journal of Glaciology*, *2*(17), 512–514. https://doi.org/10.3189/S0022143000032652

Olgin, J. G., Smith-Konter, B. R., & Pappalardo, R. T. (2011). Limits of Enceladus's ice shell thickness from tidally driven tiger stripe shear failure. *Geophysical Research Letters*, *38*(2), L02201. https://doi.org/10.1029/2010GL044950

Polashenski, C., Golden, K. M., Perovich, D. K., Skyllingstad, E., Arnsten, A., Stwertka, C., & Wright, N. (2017). Percolation blockage: A process that enables melt pond formation on first year arctic sea ice. *Journal of Geophysical Research*, *122*(1), 413–440. https://doi.org/10.1002/2016JC011994

Rudolph, M. L., Manga, M., Walker, M., & Rhoden, A. R. (2022). Cooling crusts create concomitant cryovolcanic cracks. *Geophysical Research Letters*, *49*(5), e2021GL094421. https://doi.org/10.1029/2021GL094421

Schulson, E. M., & Duval, P. (2009). *Creep and fracture of ice*. Cambridge University Press.

Shibley, N. C., & Laughlin, G. (2021). Do oceanic convection and clathrate dissocia– tion drive Europa's geysers? *Planet. Sci. J.*, *2*(6), 221. https://doi.org/10.1029/2022GL098621

Smith, R. A. (1976). The application of fracture mechanics to the problem of crevasse penetration. *Journal of Glaciology*, *17*(76), 223–228. https://doi.org/10.3198/1976JoG17-76-223-228

Smith-Konter, B., & Pappalardo, R. T. (2008). Tidally driven stress accumulation and shear failure of Enceladus's tiger stripes. *Icarus*, *198*(2), 435–451. https://doi.org/10.1016/j.icarus.2008.07.005

Tait, S., & Jaupart, C. (1992). Compositional convection in a reactive crystalline mush and melt differentiation. *Journal of Geophysical Research*, *97*(B5), 6735–6756. https://doi.org/10.1029/92JB00016

Timco, G. W., & Frederking, R. M. W. (1996). A review of sea ice density. *Cold Regions Science and Technology*, *24*(1), 1–6. https://doi.org/10.1016/0165-232X(95)00007-X

Wells, A. J., Hitchen, J. R., & Parkinson, J. R. G. (2019). Mushy-layer growth and convection, with application to sea ice. *Philosophical Transactions of the Royal Society of London, Series A*, *377*(2146), 20180165. https://doi.org/10.1098/rsta.2018.0165